Two-domains bulklike Fermi surface of Ag films deposited onto Si(111)-(7×7)

J. F. Sánchez-Royo,[1,2] J. Avila,[1,3] V. Pérez-Dieste,[1] M. De Seta,[4] and M. C. Asensio*[,1,3]
[1]*LURE, Centre Universitaire Paris-Sud, Bât. 209 D, B.P. 34, 91898 Orsay Cedex, France*
[2]*ICMUV, Dpt. Física Aplicada, Univ. de Valencia, c/Dr. Moliner 50, 46100 Burjassot, Valencia, Spain*
[3]*Instituto de Ciencia de Materiales de Madrid, CSIC, Cantoblanco, 28049 Madrid, Spain*
[4]*Dipartimento di Fisica, Università di Roma III, I-00146 Roma, Italy*
(Received 10 April 2001; revised manuscript received 19 November 2001; published 26 June 2002)

Thick metallic silver films have been deposited onto Si(111)-(7×7) substrates at room temperature. Their electronic properties have been studied by using angle-resolved photoelectron spectroscopy (ARPES). In addition to the electronic band dispersion along the high-symmetry directions, the Fermi surface topology of the grown films has been investigated. Using ARPES, the spectral weight distribution at the Fermi level throughout large portions of the reciprocal space has been determined at particular perpendicular electron-momentum values. Systematically, the contours of the Fermi surface of these films reflected a sixfold symmetry instead of the threefold symmetry of the Ag single crystal. This symmetry loss has been attributed to the fact that these films appear to be composed by two sets of domains rotated 60° from each other. Extra photoemission features at the Fermi level were also detected, which have been attributed to the presence of surface states and *sp*-quantum states. The dimensionality of the Fermi surface of these films has been analyzed, studying the dependence of the Fermi surface contours with the incident photon energy. The behavior of these contours measured at particular points along the Ag Γ*L* high-symmetry direction puts forward the three-dimensional character of the electronic structure of the investigated films.

DOI: 10.1103/PhysRevB.66.035401 PACS number(s): 73.20.−r, 71.18.+y, 79.60.−i

I. INTRODUCTION

Among the metal-Si interfaces, one of the most commonly studied systems is that of Ag films deposited onto the Si(111)-(7×7) surface reconstruction.[1] Both their fundamental and technological importances stand for the large interest in these surfaces. The 7×7 surface reconstruction is especially attractive, since its unit cell shows a reduction in the number of dangling bonds compared to the ideal 1×1 surface termination, and it shows two opposite stacking sequences, one of them having a stacking fault. Submonolayer Ag films deposited at room temperature onto Si(111)-(7×7) substrates showed that Ag preferentially condenses on the faulted halves of the 7×7 reconstruction.[2,3] As the film thickness increases, adatoms tend to cover the whole surface and, after few monolayers, multilayered three-dimensional Ag islands start to nucleate on the clusters.[4,5] Impact-collision ion-scattering spectroscopy measurements revealed that these thick Ag(111) films deposited onto Si(111)-(7×7) at room temperature consist of domains of Ag(111) crystals rotated 60° around the surface normal,[6] with their $\langle \bar{1}10 \rangle$ directions parallel to those of the substrate.[7,8]

In this context, the electronic properties of the surface develop from those of the 7×7 surface to those determined by metallic bulklike Ag films. Particularly important are the states closest to the Fermi level (E_F). They are responsible for the electron transport properties of the films as they define their Fermi surface (FS) and a potential Mott transition at low temperatures. The 7×7 surface exhibits two nearly dispersionless surface states centered at binding energies of 0.2 and 0.9 eV below the E_F.[9–12] The possible metallic behavior of this surface comes through the fact that the surface E_F is strongly pinned due to the high density of surface states near or at the E_F.[13] Nevertheless, the metallic behavior of the surface state bands close to the E_F is not yet well established.[14–16]

After deposition of the first Ag adatoms, the electronic properties of the surface are strongly modified, and conclude as bulklike thick Ag films. At the first stage of Ag deposition, valence-band spectra photoemission measurements revealed a quick suppression of the dangling-bond state of the 7×7 surface with a Ag coverage of 0.2 ML,[17] converting the surface into semiconducting.[2] Nevertheless, the increase of resistivity appears to be smaller than that expected for a suppression of the 7×7 metallic character.[18–20] As the Ag coverage increases, the surface turns to a bulklike metal, and its conductivity appears to be well described by a Drude model.[21,22] Nevertheless, this comportment has not yet been connected with the behavior of the electronic states at the E_F, that is, with the topology of the FS of these silver films. For this purpose, angle-resolved photoelectron spectroscopy (ARPES) appears to be one of the most powerful and direct tools to probe the electronic structure of solids. By directly measuring single-particle excitation spectra (also called spectral weight) as a function of momentum and energy, one can determine the most basic quantities of condensed-matter physics, e.g., the band structure, the dimensionality of electronic states, the symmetry, and quantitative analyses of the FS, electronic gap opening, nesting vector, and so forth.

In this work, we study the electronic properties and, particularly, the FS of relative thick Ag films deposited onto Si(111)-(7×7) substrates at room temperature, in order to establish the limiting coverage conditions of the work-frame in which the conductivity of Ag/Si(111)-(7×7) interfaces can be considered to be determined by metallic Ag bulklike films. This paper is organized as follows. Section II summarizes the experimental details. The results obtained by

 ©2002 The American Physical Society

ARPES are showed and discussed in Sec. III. By means of their experimental FS topology, a detailed analysis of the *quasi*-two-dimensional (*quasi*-2D) or 3D electronic character of the investigated interfaces is performed. At the end, Sec. IV is devoted to summarizing the ARPES results and focusing on the conclusions of this work.

II. EXPERIMENT

The experiments were performed at LURE (Orsay, France) using the Spanish-French (PES2) experimental station of the Super-Aco storage ring, described elsewhere.[23] The measurements were carried out in a purpose-built ultrahigh-vacuum system, with a base pressure of 5×10^{-11} mbar, equipped with an angle-resolving 50-mm hemispherical VSW analyzer coupled on a goniometer inside the chamber and a two-axes manipulator. Photoelectrons were excited with *p*-polarized synchrotron radiation in the 18–150 eV energy range. The energy resolution, obtained from the Fermi step width, was of 60–80 meV depending the photon energy. In our experiments, the incident angle of the light was fixed at 45° off normal. With this setup, the procedure to determine the FS using ARPES has been straightforward. A detailed procedure of the experimental steps was described recently by Avila and co-workers in works on electronic properties of Ag films grown on H-terminated silicon substrates and in Cu single crystal.[23,24]

The *p*-doped Si(111) single crystal substrate (with a nominal resistivity of 0.02 Ω cm) was heated up to 650 °C, in order to degas the wafer, during several hours by resistive heating and then repeatedly flashed at 1100 °C during no more than 15 sec. The structural order quality was checked out by low-energy electron-diffraction measurements (LEED), which showed sharp spots corresponding to a distinctive Si(111)-(7×7) surface reconstruction. In addition to this, no surface impurities were detected by synchrotron radiation photoemission measurements. The Si(111)-(7×7) substrate was oriented by azimuthal and polar photoelectron diffraction scans recording the Si $2p$ peak intensity.[25] Ag was evaporated onto the surface at room temperature. The evaporation rate used (of 0.06 ML/min) was determined by using a quartz microbalance. In these conditions thick Ag films, of approximately 10 ML in thickness, were deposited. In order to improve their structural quality, the samples were systematically annealed to 240 °C for 30 min. LEED spectra measured after growth revealed a clear Ag-(1×1) hexagonal pattern.

III. RESULTS AND DISCUSSION

A. Fermi-surface topology determination by using ARPES

The experimental determination of the FS of Ag by using ARPES is performed recording 2D FS cuts, which can be related to the complete 3D FS by using the photon energy dependence of the $k_\perp$. Figures 1(a) and 1(b) show the band structure diagram of Ag single crystal along the $[1\bar{1}0]$ and $[11\bar{2}]$-$[\bar{1}\bar{1}2]$ high-symmetry directions, respectively. These band dispersions have been calculated by using a tight-binding hamiltonian for fcc Ag single crystal,[26] simulating those that would be usually obtained by ARPES. In order to calculate which perpendicular electron-momentum ($k_\perp$) value was proved when $h\nu=32$ eV was used, we have assumed free-electron final states as well as a work function (Φ) value of $\Phi=4.5$ eV. With regard to the inner potential (V_o), we have considered it as a free parameter. By fitting the theoretical results to the whole set of experimental data, we have obtained a value of $V_o=-11.5$ eV, which is quite close to that early concluded by Wu *et al.* ($V_o\sim-10$ eV).[27] The Ag band diagrams of Figs. 1(a) and 1(b) show states ($E1$–$E5$ states) lying at the E_F at different parallel momentum ($k_\parallel$) values along the indicated high-symmetry directions. In essence, the experimental determination of a 2D cut of the FS by using ARPES requires scanning of the photoemission signal from states at the E_F throughout large portions of the reciprocal space. As an example of the theoretical FS cut in the $k_\parallel$ plane to be measured by using ARPES, we show in Fig. 1(c) the 2D FS cut of Ag single crystal when a photon energy of 32 eV is used to perturb the ordered

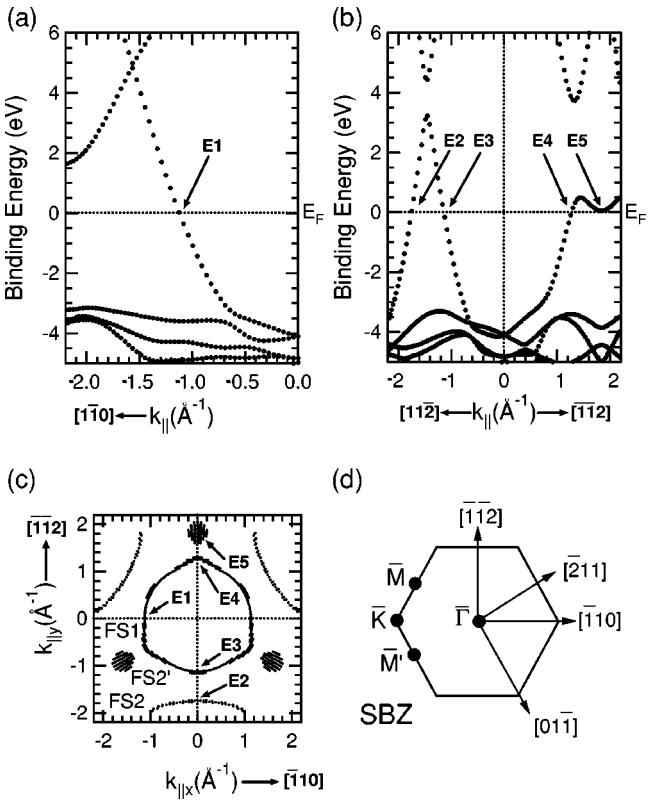

FIG. 1. Bulk Ag band dispersion calculated by using a tight-binding method along (a) the $[\bar{1}10]$ high-symmetry direction and (b) the $[\bar{1}\bar{1}2]$ and $[\bar{2}11]$ high-symmetry directions. These diagrams simulate those obtained by ARPES with $h\nu=32$ eV. States lying at the E_F are labelled from $E1$ to $E5$. (c) Corresponding Ag FS cut represented in the $k_\parallel$ plane. The different features observed have been labeled FS1, FS2, and FS2'. Points of the FS cut labeled $E1$–$E5$ correspond to states lying at the E_F indicated in (a) and (b). (d) Surface Brillouin zone of Ag(111), in which the main points and high-symmetry directions are indicated.

metallic layer.[26] This 2D FS cut is oriented as is indicated in Fig. 1(d) that shows the Ag(111) surface Brillouin zone (BZ). This 2D FS contour reflects directly the typical threefold symmetry of a fcc material. The main feature observed in this 2D FS cut can be described as a distorted ringlike feature (the FS1 feature) with a maximum value of the Fermi momentum (k_F) of $k_F = 1.29$ Å^{-1} along the $\langle \overline{112} \rangle$ directions, a value of $k_F = 1.17$ Å^{-1} along the $\langle \overline{2}11 \rangle$ directions, and a minimum value of $k_F = 1.13$ Å^{-1} along the $\langle \overline{1}10 \rangle$ directions. According to the BZ extended zone scheme, additional cuts of FS in neighboring BZ's are also expected along the $\langle \overline{2}11 \rangle$ directions (FS2 features) as well as along the $\langle \overline{112} \rangle$ directions (FS2' features).

In the following, we emphasize the ability of the ARPES technique to determine *in situ* FS contours throughout all the BZ directions. This ability allows us to focus a detailed study of the electronic states near the Fermi level at particular portions of the reciprocal space. The photoemission process involves energy and crystal momentum conservation. In the framework of the three-step model of the photoexcitation mechanism in ARPES, the momentum of the electrons inside a bulk material can be determined. In this case, both momentum components $k_\parallel$ and $k_\perp$ of photoexcited electrons from states at the E_F can be expressed as[28]

$$k_\parallel = \sqrt{\frac{2m}{\hbar^2}} \sqrt{h\nu - \Phi} \sin(\Theta_{off}) \tag{1a}$$

and

$$k_\perp = \sqrt{\frac{2m}{\hbar^2}} \sqrt{(h\nu - \Phi)\cos^2(\Theta_{off}) - V_o}, \tag{1b}$$

where m is the free-electron mass and $\hbar$ is the reduced Planck constant. These equations directly imply that, using a constant $h\nu$, all the initial states with a spherical shell $(k_\parallel, k_\perp)$ of the BZ are probed. Figure 2 shows a transversal cut of the bulk Ag BZ in the extended zone scheme. This schematic view corresponds to the cut of the Ag BZ by the plane defined by the [111] and $[\overline{2}11]$ high-symmetry directions. The most important points are also indicated. The intersection of the Ag FS of contiguous BZs with that plane is also shown, which forms the so-called dog-bone contours. In the figure, successive spherical shells have been indicated throughout the bulklike Ag FS by using Eqs. (1) for $h\nu = 32$, 55, and 96 eV. They have been calculated for Θ_{off} values ranging between 0° and 55°, which correspond to our typical experimental conditions. The intersection between the Ag FS and these shells defines 2D FS contours, which pass close to the middle between the Γ and L points for $h\nu = 32$ eV, near the L point for $h\nu = 55$ eV, and near the Γ point for $h\nu = 96$ eV.

B. Fermi surface of 10-ML Ag(111) films grown on Si(111)-(7×7) substrates

Figure 3 shows the experimental 2D FS cut measured in 10-ML-thick Ag films using light of $h\nu = 32$ eV. Photoelectron angular distribution measurements are indicated by taking the *x*-axis as the $[\overline{1}10]$ direction of the crystal. The identification of the high-symmetry directions of the surface by LEED measurements before and after the Ag deposition allows us to confirm that the Ag(111) films onto Si(111)-(7×7) grow epitaxially with the Ag overlayer $\langle \overline{1}10 \rangle$ high-symmetry directions parallel to those of the the Si substrate, as previously reported.[7,8] The image has been scaled in such a way that it is linear in photoemission intensity and in $k_\parallel$. Only the central part of the image ($k_\parallel < 0.4$ Å^{-1}) was background-enhanced by a constant factor of 2, in order to appear visible in the image. The photoemission intensity is maximum for the brightest feature and minimum for the darkest one. In this image, well-defined features can be observed, indicating the momentum distribution of initial states lying at the E_F as a function of $k_\parallel$.

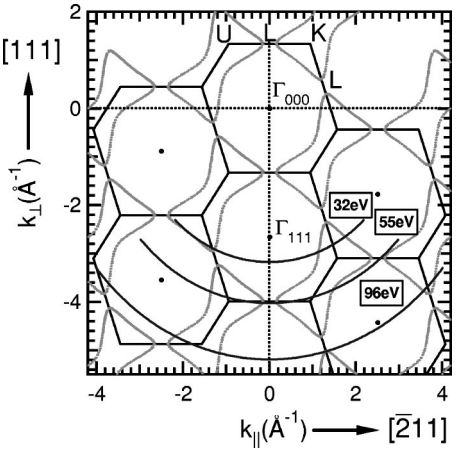

FIG. 2. Intersection of final-state nearly free electron spheres for $h\nu = 32$, 55, and 96 eV, with the typical polygons of the Ag Brillouin zone in two selected directions. The so-called dog-bone structures of the FS cross section in the selected plane are also shown. Notice that, by changing $h\nu$, the whole three-dimensional Brillouin zone can be studied.

The experimental photoelectron spectral weight image at the E_F (Fig. 3) exhibits most of the characteristic features predicted for a FS of a bulklike Ag single crystal [Fig. 1(c)]. Nevertheless, the experimental FS contour shows a sixfold rather than the typical threefold symmetry of the FS contour of bulklike fcc Ag single crystal. This clear result is a consequence of the two-domain character of the Ag films grown onto Si substrates, which can also be confirmed by diffraction techniques. Forward scattering photoelectron diffraction (PhD) has recently demonstrated that the metallic films grow epitaxially oriented with respect to the substrate, and that the overlayer consists of two domains of fcc Ag lattices rotated 60° from each other.[29] As PhD is a technique that takes into account photoelectrons from all the adatoms at the interface, we have two independent contributions to the photoelectron signal from the two coexisting metallic domains. Therefore, the photoelectrons with $k_\parallel$ corresponding to $[\overline{2}11]$ and $[\overline{112}]$ directions of two inequivalent domains will overlap in the recorded photoemission signal. Figure 3(b) shows the theoretical Ag FS cut calculated for two domains rotated 60°

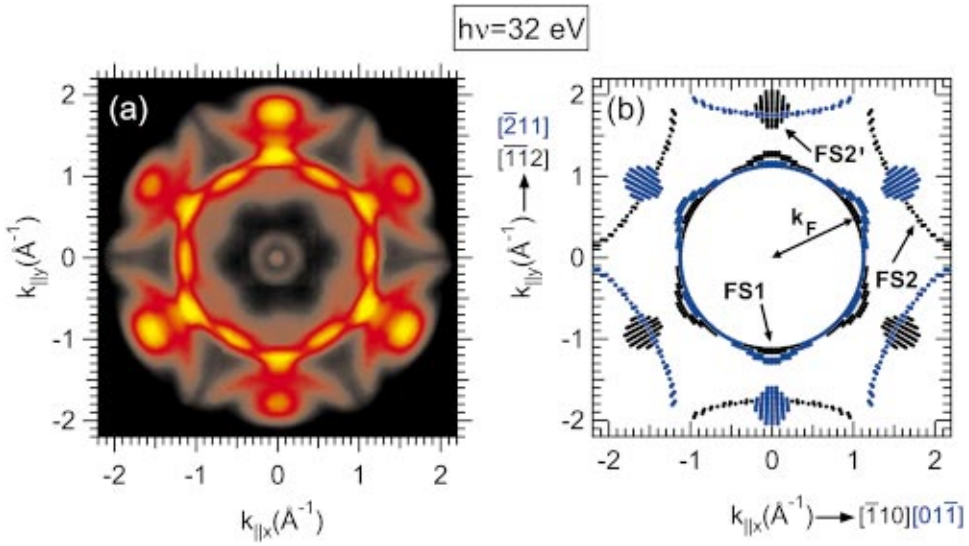

FIG. 3. (Color) (a) Spectral weight at the E_F measured by ARPES with $h\nu=32$ eV in a thick Ag film deposited onto Si(111)-(7×7). (b) Ag Fermi-surface cut represented in the $k_\parallel$ plane as calculated by using a tight-binding method for $h\nu=32$ eV, and corresponding to a film composed with two 60°-rotated domains. The FS cuts of both domains are indicated by different colors.

for $h\nu=32$ eV, in which, for simplicity, only features appearing in the FS cut of one of the domains are indicated. As one can see, these results are in excellent agreement with the experimental data shown in Fig. 3(a).

In order to carry out a more quantitative analysis of the spectral weight images as obtained by ARPES, we have followed the gradient procedure proposed by Straub *et al.*[30] It involves the calculation of the gradient of the FS images ($|\nabla_{k_\parallel} w(k_\parallel)|$), $w(k_\parallel)$ being the spectral weight measured at the E_F). This procedure produces two maxima out of each maximum of the spectral weight at the E_F [Fig. 3(a)]. It was found that, out of the two maxima of the gradient, the one on the unoccupied side of the band crossing the E_F accurately reflects the $k_\parallel$ values of the FS cuts.

Analyzing the measured spectral weight image by this method, we have obtained the gradient of the image showed in Fig. 3(a). This is displayed in Fig. 4, together with the two-domain Ag FS cut calculated for $h\nu=32$ eV [Fig. 3(b)]. The FS1, FS2, and FS2' features labeled in Fig. 4 are fairly reproduced by the calculated Ag FS cut. Only the FS2 feature obtained by calculations is shifted by ΔFS2$=0.3$ Å^{-1} with respect to the experimental data. Nevertheless, this is not surprising since our calculations are not fully relativistic, and neither final-state nor many-body effects have been considered, which have shown to play an important role in band structure calculations in the related fcc Cu metal.[31,32]

Figure 5 shows the profile of both the spectral weight at the E_F measured with $h\nu=32$ eV and its gradient along the $\langle\bar{1}10\rangle$ directions [Fig. 5(a)] and along the $\langle\bar{1}\bar{1}2\rangle$ and $\langle\bar{2}11\rangle$ overlapped directions [Fig. 5(b)]. Following the Straub *et al.*'s procedure,[30] we have obtained average values of $k_F=1.21\pm0.06$ Å^{-1} along the $\langle\bar{1}10\rangle$ directions and $k_F=1.34\pm0.06$ Å^{-1} along the $\langle\bar{1}\bar{1}2\rangle$ and $\langle\bar{2}11\rangle$ directions. These experimental values are in concordance with those obtained by tight-binding calculations showed in Fig. 1(c).

Whereas the 2D Ag FS cut for $h\nu=32$ eV in contiguous BZs is correctly reproduced by the results of tight binding, there are some particular experimental features that are not theoretically predicted. Figure 4 shows the presence of *s* and *h* features. The *s* feature appears as a rather diffuse ringlike feature at ~0.26 Å^{-1} with an intense spot at the center of the image of 0.10 Å^{-1} in radius. The *h* feature is a diffuse fluted contour at $k_\parallel\sim0.7$ Å^{-1} that appears under the FS cut in the first BZ in the $\langle\bar{1}\bar{1}2\rangle$ and $\langle\bar{2}11\rangle$ directions, and seems to connect points of the FS cut in the $\langle\bar{1}10\rangle$ directions.

In order to analyze the behavior of these unexpected features, we have measured the band dispersion of the Ag films along the $[\bar{1}10]$ direction and along the $[\bar{1}\bar{1}2]$ and $[\bar{2}11]$ coincident directions. Figures 6(a) and 6(b) show the spectra obtained along these high-symmetry directions, respectively. We have centered our attention in occupied states whose binding energy is up to 3 eV below the E_F. In these figures,

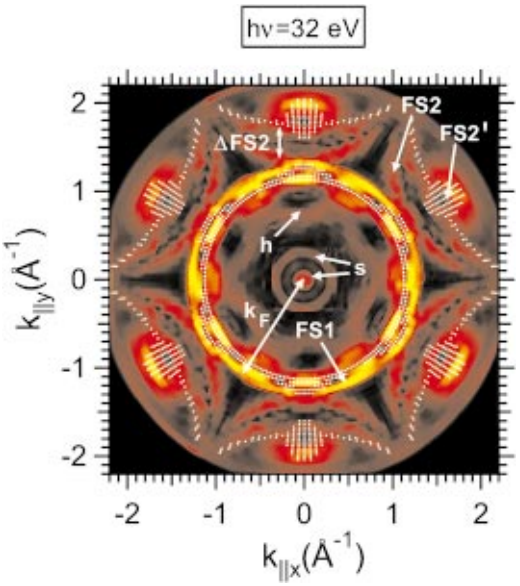

FIG. 4. (Color) Gradient of the spectral weight at the E_F shown in Fig. 3(a). The Fermi surface cut calculated for $h\nu=32$ eV in the case of a Ag film with 60°-rotated domains is also plotted by dotted lines. The different features observed and the Fermi vector are indicated. The misfit in the position of the FS2 feature is also indicated (ΔFS2).

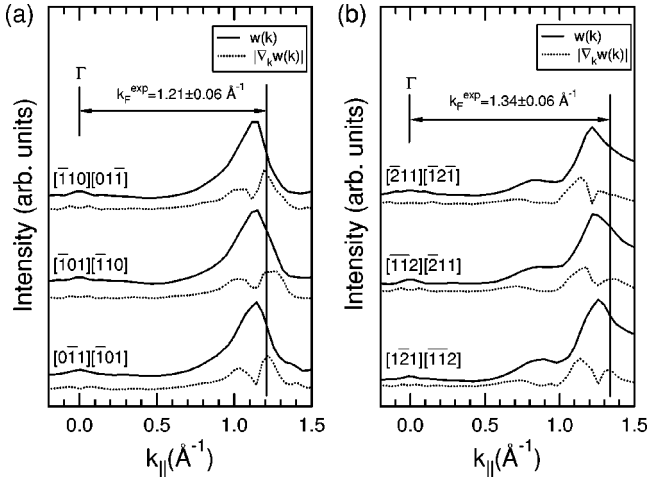

FIG. 5. Spectral weight at the E_F measured in (a) the $\langle\bar{1}10\rangle$ overlapped direction and (b) the $\langle\bar{1}\bar{1}2\rangle$ and $\langle\bar{2}11\rangle$ overlapped directions (solid curves). The gradient of each profile is also plotted under the corresponding direction by dotted curves. The value of k_F extracted from these gradients is drawn as the average value. Its position is marked by a solid vertical bar.

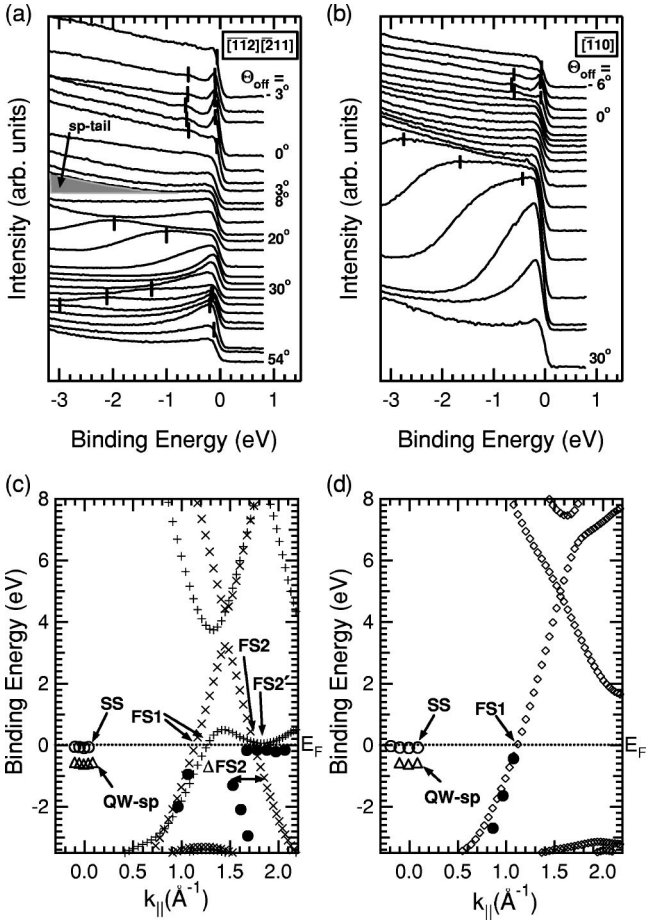

FIG. 6. Energy distribution curves measured in a thick Ag film with $h\nu=32$ eV along (a) the overlapped $[\bar{1}\bar{1}2]$ and $[\bar{2}11]$ symmetry directions and (b) the $[\bar{1}10]$ symmetry direction. The binding energy origin of these curves is taken at the E_F. The value of Θ_{off} is given for some of the curves, the rest of them being equally Θ_{off} separated between two consecutively labeled curves. The different peaks identified have been marked by small solid bars. A dashed area in the $\Theta_{off}=14°$ curve has been labelled as the *sp tail*. (c) and (d) (Circles, full circles, triangles) band dispersion diagram extracted from the peaks identified in (a) and (b), respectively. (crosses, plus, diamonds) band dispersion calculated with $h\nu=32$ eV along the $[\bar{1}\bar{1}2]$, $[\bar{2}11]$, and $[\bar{1}10]$ symmetry directions, respectively. The E_F position is marked by dotted lines. Bulk states of the calculated bands lying at E_F are labeled as in Fig. 3(b).

we have identified different photoemission peaks which are indicated by solid bars. The binding energy of the identified states is plotted versus $k_{||}$ for both symmetry directions in Figs. 6(c) and 6(d), respectively. Band dispersion calculations corresponding to these symmetry directions for $h\nu=32$ eV have been also included in these figures.[26] In the range of binding energy close to the E_F, the band dispersion of the occupied *sp* band is the only noticeable structure. In our ARPES measurements, the *sp* band dispersion in the first BZ appears unresolved for both $[\bar{1}\bar{1}2]$ and $[\bar{2}11]$ directions [Figs. 6(a) and 6(c)]. The different states of the *sp* band, particularly near the E_F, are those defining the FS1, FS2, and FS2' features observed in Fig. 4. In particular, it should be noticed that the shift of the FS2 feature of 0.3 Å^{-1} at the E_F [Fig. 6(c)] is also observed in the occupied *sp* band up to 3 eV below the E_F.

The two occupied states which are not reproduced by the bulklike Ag band structure are those appearing at normal emission labeled as *SS* and *QW-sp* in Figs. 6(c) and 6(d) with binding energies of 0.09 and 0.64 eV, respectively. On the one hand, the *SS* feature can be attributed to the well-known Shockley surface state located in the *sp* band gap at the *L* point of the bulk BZ,[33] whose existence has been attributed to the break of crystalline periodicity at the surface.[34] The proximity of this state to the E_F means that the central spot of the *s* feature observed in Fig. 4 can be attributed to emission at the E_F from this surface state. On the other side, the *QW-sp* feature can be attributed to an *sp*-quantum state. Quantum states have been early observed in ARPES measurements in 5–15-ML Ag films deposited onto Si(111)-(7×7) substrates,[35] which have been identified as film states associated with the confinement of the *sp* band of bulk Ag. In the framework of the phase accumulation model, the binding energy of confined states depends on film thickness and on the reflection at the interface.[36] In our 10-ML Ag films, a perpendicular confinement of the *sp* states produces confined film states with a minimum binding energy of 0.6 eV. Nevertheless, no trace from confined states with a higher quantum number (n) than $n=1$ has been detected in our measurements, which can be attributed to film-thickness inhomogeneities. In any case, this confined state is observed, as expected, to disperse parabolically through the E_F. Outside of normal emission, the signal from this state tends to vanish due to the loss of coherence. Nevertheless, this state becomes close enough to the E_F to produce the ringlike *s* feature of ~0.26 Å^{-1} in radius, observed in Fig. 4.

The behavior of the *h* feature observed in Fig. 4 is rather different from that observed for the *s* features. The cuts of

the E_F of the sp band, as shown in Figs. 6(c) and 6(d), appear at the $k_\parallel$ values observed in the FS cut with $h\nu = 32$ eV (Fig. 4). Nevertheless, in Figs. 6(a) and 6(b), no trace of any occupied band appears close to the E_F in the spectra measured to 15° off-normal, corresponding to $k_\parallel \sim 0.7$ Å^{-1}. In these spectra, one can only see the trace of a wide tail of the sp band that lies close to the E_F and whose maximum appears 4 eV below it [shadow area in Fig. 6(a)]. The presence of the wide tail of the sp band extending just below the E_F has also been observed in Ag(111) and in Cu(100) single crystal by photoemission measurements in normal emission with $h\nu = 7$–9 and 21.2 eV and with $h\nu = 12$–14 eV, respectively.[37–39] This fact has been attributed to indirect transitions induced by the surface. Moreover, this large tail of the sp band is expected mostly to reflect the p-like behavior of deeper sp states. Therefore, the presence of the fluted contour in the 2D FS image of Fig. 4 can be attributed to a consequence of the surface perturbation process involved in the photoemission technique.

C. Two- or three-dimensional behavior of the Fermi surface of thick Ag(111) films grown on Si substrates

In order to continue the study on the electronic properties of thick Ag films grown on Si(111)-(7×7) substrates we have centered our further analysis on the 2D or 3D behavior of the FS of these films. This question was approached in an early work by analyzing the d-valence-band dispersion of Ag films grown onto Cu(001) single crystal.[40] In that work, photoemission measurements revealed that the d band shows already a 3D band dispersion for Ag films of 3–5 ML in thickness. The radial extent of d states confines their interactions to nearest neighbors, and this interaction is strongly screened by the sp electrons. Nevertheless, the sp states extend to additional neighboring sites. These facts would explain the 3D behavior of the deeper d bands in very thin films, but they would not necessary imply the same behavior for the FS of such a thin Ag films. A bulklike behavior of the FS has also been observed in 1 ML Ni films on Cu(001).[41] In this case, the 3D behavior of the sp band has been attributed to the short screening length of electrons in metals and to a strong hybridization between the Ni sp-d_{z^2} hybrid and the Cu sp, both of them crossing the E_F. Through that hybridization, the Bloch periodicity of the substrate is imposed on the electronic wave functions of the film. In Ag films deposited onto semiconducting Si(111)-(7×7) substrates the sp states at the E_F have a strong screening effect inside the substrate. Therefore, the evolution from a 2D to a 3D Ag FS would come from the fulfillment of periodicity condition of the sp wave functions inside the films.

The different dimensionality of the metallic films can be clearly elucidated by using a tuneable light source. Let us consider the limit case of thin films with 2D electronic properties. In this case, electronic states have a definite $k_\parallel$, whereas their $k_\perp$ is undefined, since the overlayer has not enough periodicity to ensure crystal momentum conservation in the perpendicular direction. In particular, in the frame of the nearly free-electron model, the FS of 2D Ag(111) metallic films would be expected to be ringlike with the ring axis parallel to the [111] surface vector and contained in the surface BZ. In this case, the FS cuts measured with different incident photon energy show FS features placed at the same $k_\parallel$ values, independently of $h\nu$. Opposite to this, in the case of thin metallic Ag films with 3D electronic properties both $k_\parallel$ and $k_\perp$ depend on the photon energy, defined as indicated in Eqs. (1). Therefore, measurements of the cross-sectional cuts of the FS with different $h\nu$ will indicate a clear dependence on $k_\perp$. The analytical relation between the photon energy and $k_\perp$ allow us to scan the bulklike Ag FS (Fig. 2) using different $k_\perp$ values, (i.e., by changing the photon energy).

Figures 7(a) and 7(b) show the spectral weight distribution at the E_F measured in a thick Ag film deposited onto Si(111)-(7×7) with $h\nu = 55$ and 96 eV, respectively. These images have been plotted in the same conditions as those exposed in Fig. 3(a). All the FS contours measured at different $h\nu$ exhibit the sixfold symmetry expected for a two-domain Ag film. Using photon energies of $h\nu = 55$ and 96 eV, the FS cuts through the first scanned BZ appear as a central bright spot, with a radius of 0.16 ± 0.08 Å^{-1}, and a ringlike feature, respectively. The FS cuts in contiguous BZ's also show different features as $h\nu$ increases. No trace from surface states can be distinguished in the $h\nu = 55$ and 96 eV images. The fact that the features corresponding to the Ag FS change in the $k_\parallel$ plane with increasing $h\nu$ suggests the presence of bulklike electronic states with a clear 3D character.

To perform a quantitative analysis of the measured FS contours, we have calculated the gradient of the spectral weight at the E_F images of Figs. 7(a) and 7(b), following the procedure suggested by Straub *et al.*[30] Figures 7(c) and 7(d) show the results of these calculations for $h\nu = 55$ and 96 eV, respectively. We have also included in these figures the cuts of the bulklike Ag FS calculated for a film composed with 60°-rotated domains corresponding to the momentum space probed with $h\nu = 55$ and 96 eV. These plots fairly agree with the experimental results. These facts, together with those of Fig. 4, definitively put forward the 3D behavior of the FS of 10-ML Ag films deposited onto Si(111)-(7×7) substrates. In this sense, the electronic properties of Ag films of similar thicknesses, deposited onto different substrates, should show a similar bulklike FS, as occurs in films deposited onto H-passivated Si(111)-(1×1) surfaces.[24] Only states related to the film surface (surface and quantum states) may show some differences.[24,42]

These results also point out that parameters defining the FS of these Ag films can be compared to those corresponding to bulklike Ag single crystal. In order to simultaneously determine k_F and other characteristic parameters of a 3D FS in different symmetry directions, it should be taken into account that the measured k_F values are $k_\perp$ dependent.[43] Therefore, the reliability of the deduced values also depends on a good $k_\perp$ determination. In our case, the good concordance obtained in the determination of the Ag FS in the first BZ for all $h\nu$ used in this work suggest that $k_\perp$ is reasonably well determined by a constant inner potential $V_0 = -11.5$ eV. In any case, the influence of V_o on the determination of a bulk-

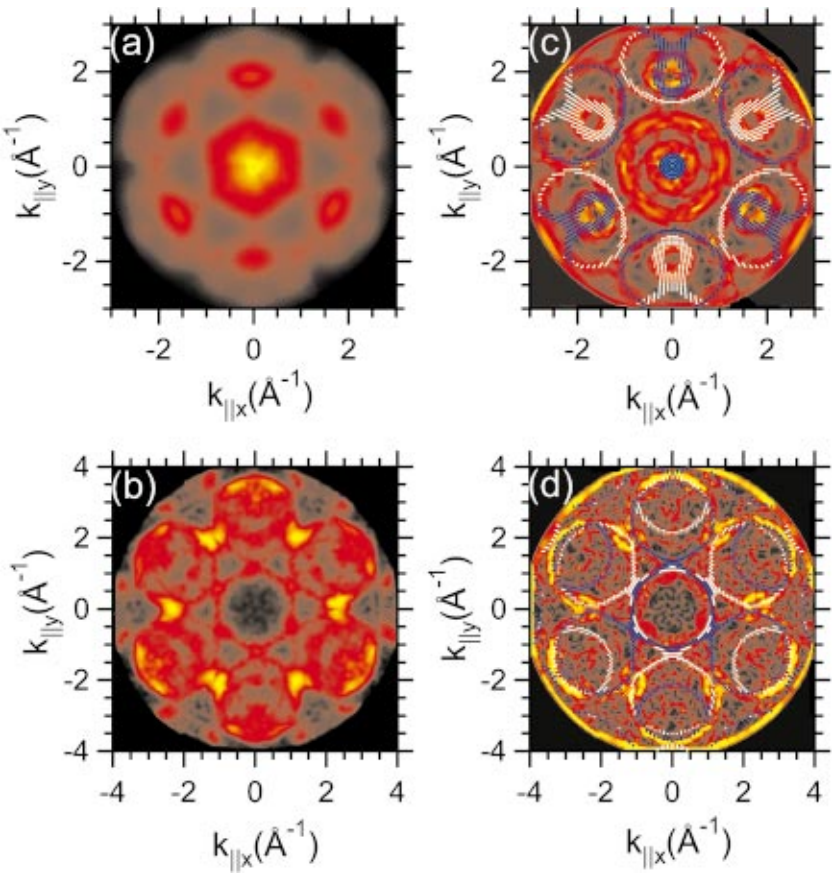

FIG. 7. (Color) (a) and (b) Spectral weight at the E_F measured by ARPES with $h\nu=55$ and 96 eV, respectively, in a thick Ag film deposited onto Si(111)-(7×7). (c) and (d) Gradient of the spectral weight images shown in (a) and (b), respectively. The corresponding Fermi-surface cuts calculated for $k_{\|}$ areas probed with $h\nu=55$ and 96 eV are also plotted (dotted lines). The fact that films are composed of two domains has been considered in these calculations (the FS cuts for each domain are showed by different colors).

like 3D FS can be overcame with an exhaustive determination of the Ag FS in a well-defined range of $h\nu$.

From our results, on the one hand, we can directly estimate the *neck* radius of the Ag FS at the L point from the spectral weight at the E_F image measured with $h\nu=55$ eV, which appears to be 0.16 ± 0.08 $Å^{-1}$. This value of the *neck* radius of the Ag FS is in good agreement with those obtained from other methods.[44–46] On the other hand, in Sec. IV we have estimated the k_F values for different parallel to the surface symmetry directions. As the FS of these films appears to show a 3D behavior, these values of k_F can be also compared with those obtained in Ag single crystal by the Haas-Van Alphen method [$k_F(\Gamma X)=1.258$ $Å^{-1}$) and those determined by ARPES measurements in quantum-well sp-states in Ag(100) films [$k_F(\Gamma X)=1.272\pm0.002$ $Å^{-1}$).[44,47] In spite of the small discrepancy between these two precedent estimates of k_F, they can be considered comparable, since the high precision of the latter refers to statistical deviations, without considering the accuracy of the model used.[47] The fact that our estimate of k_F appears to be slightly lower than the previous ones can be attributed to the fact that our measurements do not exactly probe the FS cut in the ΓX direction (Fig. 4). A simple geometrical calculation (Fig. 4) will let us estimate $k_F(\Gamma X)=1.27\pm0.06$ $Å^{-1}$, which is in agreement with those estimates of k_F.

Finally, it should be pointed out that the 3D electronic behavior of the FS of Ag films grown onto Si(111)-(7×7) substrates establishes the workframe in which the determination of the transport properties of such a thick films can be carried out. Our results show that, besides scattering mechanisms involved in electronic transport, electronic states contributing to current can be assumed to be very similar to those characteristic of the bulk metallic material. Therefore, conductivity and transport properties of these films are expected to be mainly determined by impurity, phonon, and defectlike scattering mechanisms of electrons at the E_F with transport parameters close to those of a single crystal material. In fact, conductivity and magnetoconductivity measurements carried out in 10-ML Ag films deposited onto Si(111)-(7×7) substrates at low temperature show a temperature dependence of resistance well described by a Drude model, with a linear coefficient at temperatures higher than 40 K close to that of single crystals.[21,22] These results appear to contrast with plasmon frequency measurements by energy-loss spectroscopy LEED carried out in up to 18-ML Ag films deposited onto Si(111)-(7×7) substrates at different temperatures.[48] In these measurements, plasmon confinement effects into single domains were attributed to lateral extent of grains rather than to a perpendicular confinement in the films, in spite of the metallic conductivity behavior observed in those films. The mean free path of electrons in those films is around some tens of $Å^{-1}$, at low temperature,[21] which is of the order of lateral extension of the grains.[48] These facts suggest that strong lateral confinement effects are expected mostly to appear in thinner films, as revealed by magnetoconductivity measurements,[22] since they show a higher granular density. In this context, ac conductivity measurements or high-magnetic-field conductivity measurements

at low temperature rather than dc conductivity measurements in 10-ML Ag films are expected to show lateral confinement effects. In any case, the fact that films appear to be composed by two 60°-rotated domains may smooth grain boundary scattering mechanisms due to strong hybridization of sp states at grain boundaries. This fact would favor that mean free path of electrons is mainly determined by film thickness rather than grain size effects of such a thin films.

IV. SUMMARY AND CONCLUSIONS

Thick Ag films have been deposited onto Si(111)-(7×7) substrates at room temperature. The electronic properties of these films have been studied by measurements of spectral weight at the E_F at different $h\nu$. With this technique, cross-sectional cuts of the FS of these films have been obtained for particular values of $k_\perp$. The FS cuts measured in these films reflect clear features with a sixfold symmetry. In order to analyze this result, we have compared the experimental FS cuts with theoretical FS cuts of a 3D Ag single crystal. The calculated Ag FS cuts fairly well reproduces most of the features observed in the experimental data, but the sixfold symmetry of the Ag films FS is not reproduced. These facts suggest that the loss of symmetry order of these Ag films is due to their structural composition. In fact, the Ag FS calculated for films composed with two domains rotated 60° fairly well reproduces the experimental FS cuts of these films in the whole space of the BZ analyzed.

In addition to this, photoemission traces at the E_F not belonging to a bulklike Ag FS have been also detected in the FS of these thick Ag films. They have been attributed to the presence of surface states, which are located in the sp band gap at the L point of the BZ, and to sp-quantum states of these films. Also, additional features have been detected coming from the tail of deep sp states.

The fact that the FS contours of thick Ag films are well reproduced by bulklike Ag FS cut for a particular $k_\perp$ value encouraged us to determine the dimensionality of the FS of these films. In order to solve this point, FS mapping was carried out by measuring Ag FS cuts with different photon energies. The FS contours measured at $h\nu=32$, 55, and 96 eV reflect different traces of the FS as $h\nu$ increases, which puts forward the 3D behavior of the FS of these films. The bulklike Ag FS cuts calculated for films composed by two domain, with $k_\perp$ values corresponding to $h\nu=32$, 55, and 96 eV, fit the FS cuts of these thick Ag films in the whole BZ scanned.

ACKNOWLEDGMENTS

This work was financed by DGICYT (Spain) (Grant No. PB-97-1199) and the Large Scale Facilities program of the EU to LURE. J.F.S.-R. and V. P.D. acknowledge financial support from the Ministerio de Educación y Cultura of Spain.

*Electronic address: asensio@lure.u-psud.fr

[1] S. Hasegawa, X. Tong, S. Takeda, N. Sato, and T. Nagao, Prog. Surf. Sci. **60**, 89 (1999).
[2] St. Tosch and H. Neddermeyer, Phys. Rev. Lett. **61**, 349 (1988).
[3] A. Shibata, Y. Kimura, and K. Takayanagi, Surf. Sci. **303**, 161 (1994).
[4] K.J. Wan, X.F. Lin, and J. Nogami, Phys. Rev. B **47**, 13 700 (1993).
[5] Z.H. Zhang, S. Hasegawa, and S. Ino, Phys. Rev. B **55**, 9983 (1997).
[6] K. Sumitomo, K. Tanaka, Y. Izawa, I. Katayama, F. Shoji, K. Oura, and T. Hanawa, Appl. Surf. Sci. **41-42**, 112 (1989).
[7] Y. Gotoh, S. Ino, and H. Komatsu, J. Cryst. Growth **56**, 498 (1982).
[8] Y. Gotoh and S. Ino, Thin Solid Films **109**, 255 (1983).
[9] J.E. Rowe and H. Ibach, Phys. Rev. Lett. **32**, 421 (1974).
[10] F. Houzay, G.M. Guichar, R. Pinchaux, P. Thiry, Y. Petroff, and D. Dagneaux, Surf. Sci. **99**, 28 (1980).
[11] F.J. Himpsel, D.E. Eastman, P. Heimann, B. Reihl, C.W. White, and D.M. Zehner, Phys. Rev. B **24**, 1120 (1981).
[12] R.I.G. Uhrberg, T. Kaurila, and Y.-C. Chao, Phys. Rev. B **58**, R1730 (1998).
[13] F.J. Himpsel, G. Hollinger, and R.A. Pollak, Phys. Rev. B **28**, 7014 (1983).
[14] R. Schad, S. Heun, T. Heidenblut, and M. Henzler, Phys. Rev. B **45**, 11 430 (1992).
[15] D. Fick, R. Veith, H.D. Ebinger, H.J. Jänsch, C. Weindel, H. Winnefeld, and J.J. Paggel, Phys. Rev. B **60**, 8783 (1999).
[16] R. Losio, K.N. Altmann, and F.J. Himpsel, Phys. Rev. B **61**, 10 845 (2000).
[17] A. Samsavar, T. Miller, and T.-C. Chiang, Phys. Rev. B **42**, 9245 (1990).
[18] M. Henzler, in *Surface Physics of Materials I*, edited by J.M. Blakely (Academic, New York, 1975), p. 241.
[19] Y. Hasegawa, I.-W. Lyo, and P. Avouris, Surf. Sci. **357-358**, 32 (1996).
[20] S. Heike, S. Watanabe, Y. Wada, and T. Hashizume, Phys. Rev. Lett. **81**, 890 (1998).
[21] M. Henzler, T. Lüer, and A. Burdach, Phys. Rev. B **58**, 10 046 (1998).
[22] M. Henzler, T. Lüer, and J. Heitmann, Phys. Rev. B **59**, 2383 (1999).
[23] J. Avila, C. Casado, M.C. Asensio, J.L. Pérez, M.C. Muñoz, and F. Soria, J. Vac. Sci. Technol. A **13**, 1501 (1995).
[24] A. Arranz, J.F. Sánchez-Royo, J. Avila, V. Pérez-Dieste, P. Dumas, and M.C. Asensio, Phys. Rev. B **65**, 075405 (2002).
[25] A. Mascaraque, J. Avila, C. Teodorescu, M.C. Asensio, and E.G. Michel, Phys. Rev. B **55**, R7315 (1997).
[26] D.A. Papaconstantopoulos, *Handbook of the Band Structure of Elemental Solids* (Plenum, New York, 1986). The band diagrams have been calculated with an empirical second-neighbor tight-binding Hamiltonian. The orthogonal two-center tight-binding parameters given by Papaconstantopoulos have been used.
[27] S.C. Wu, H. Li, J. Sokolov, J. Quinn, Y.S. Li, and F. Jona, J. Phys.: Condens. Matter **1**, 7471 (1989).
[28] S. Hüfner, *Photoelectron Spectroscopy*, Springer Series in Solid-State Sciences Vol. 82 (Springer-Verlag, Berlin, 1995).
[29] V. Pérez-Dieste J.F. Sánchez-Royo, J. Avila, and M.C. Asensio (unpublished).

[30] Th. Straub, R. Claessen, P. Steiner, S. Hüfner, V. Eyert, K. Friemelt, and E. Bucher, Phys. Rev. B **55**, 13 473 (1997).
[31] V.N. Strocov, R. Claessen, G. Nicolay, S. Hüfner, A. Kimura, A. Harasawa, S. Shin, A. Kakizaki, P.O. Nilsson, H.I. Starnberg, and P. Blaha, Phys. Rev. Lett. **81**, 4943 (1998).
[32] A. Marini, G. Onida, and R. Del Sole, Phys. Rev. B **64**, 195125 (2001).
[33] J.G. Nelson, S. Kim, W.J. Gignac, R. S. Williams, J.G. Tobin, S.W. Robey, and D.A. Shirley, Phys. Rev. B **32**, 3465 (1985).
[34] P.M. Echenique and J.B. Pendry, J. Phys. C **11**, 2065 (1978).
[35] A. L. Wachs, A.P. Shapiro, T.C. Hsieh, and T.-C. Chiang, Phys. Rev. B **33**, 1460 (1986).
[36] N.V. Smith, N.B. Brookes, Y. Chang, and P.D. Johnson, Phys. Rev. B **49**, 332 (1994).
[37] T. Miller, W.E. McMahon, and T.-C. Chiang, Phys. Rev. Lett. **77**, 1167 (1996).
[38] T. Michalke, A. Gerlach, K. Berge, R. Matzdorf, and A. Goldmann, Phys. Rev. B **62**, 10 544 (2000).
[39] E.D. Hansen, T. Miller, and T.-C. Chiang, Phys. Rev. Lett. **78**, 2807 (1997).
[40] J.G. Tobin, S.W. Robey, L.E. Klebanoff, and D.A. Shirley, Phys. Rev. B **28**, 6169 (1983).
[41] G.J. Mankey, K. Subramanian, R.L. Stockbauer, and R.L. Kurtz, Phys. Rev. Lett. **78**, 1146 (1997).
[42] G. Neuhold and K. Horn, Phys. Rev. Lett. **78**, 1327 (1997).
[43] P. Aebi, J. Osterwalder, R. Fasel, D. Naumović, and L. Schlapbach, Surf. Sci. **307-309**, 917 (1994).
[44] P.T. Coleridge and I.M. Templeton, Phys. Rev. B **25**, 7818 (1982).
[45] A.H. McDonald, J.M. Daams, S.H. Vosko, and D.D. Koelling, Phys. Rev. B **25**, 713 (1982).
[46] G. Fuster, J.M. Tyler, N.E. Brener, J. Callaway, and D. Bagayoko, Phys. Rev. B **42**, 7322 (1990).
[47] J.J. Pagel, T. Miller, and T.-C. Chiang, Phys. Rev. B **61**, 1804 (2000).
[48] F. Moresco, M. Rocca, T. Hildebrandt, and M. Henzler, Phys. Rev. Lett. **83**, 2238 (1999).